Existence and Bifurcation of Canards in $\mathbb{R}^3$ in the case of a Folded Node

Martin Wechselberger*
Mathematical Biosciences Institute, Ohio State University,
231 West 18th Ave, Columbus, OH 43210, USA
E-mail: wm@mbi.osu.edu

Abstract

We give a geometric analysis of canards of folded node type in singularly perturbed systems with 2-d folded critical manifold using the blow-up technique. The existence of two primary canards is well known provided a generic non-resonance condition $\mu \notin \mathbb{N}$ is satisfied. We show that due to resonances bifurcation of secondary canards occur. We give a detailed geometric explanation for this phenomenon using an extension of Melnikov-theory to prove a transcritical bifurcation of canards for odd μ. Furthermore we show numerically the existence of a pitchfork bifurcation for even μ and a novel turning point bifurcation close to $\mu \in \mathbb{N}$. We conclude the existence of $[(\mu-1)/2]$ secondary canards away from the resonances. Finally we apply our results to a network of HH neurons with excitatory synaptic coupling and explain the observed slowing of the firing rate of the synchronized network due to the existence of canards of folded node type.

1 Introduction

We consider three-dimensional systems of singularly perturbed ordinary differential equations in standard form

$$\begin{aligned} \dot{x} &= g_1(x,y,z,\varepsilon) \\ \dot{y} &= g_2(x,y,z,\varepsilon) \\ \varepsilon\dot{z} &= f(x,y,z,\varepsilon)\,, \end{aligned} \tag{1}$$

with sufficiently smooth functions g_1, g_2, f and small parameter $0<\varepsilon\ll 1$. The variables $(x,y)\in\mathbb{R}^2$ are slow variables, $z\in\mathbb{R}$ is a fast variable. The independent variable is the slow time τ. Taking the limit $\varepsilon\to 0$ in system (1) we obtain the reduced problem on the critical manifold $S:=\{(x,y,z)\in\mathbb{R}^3 \,:\, f(x,y,z,0)=0\}$. We assume that the critical manifold S is a nondegenerate folded surface in a neighbourhood of the origin. Sufficient conditions for this assumption are:

$$\begin{aligned} &f(0,0,0,0)=0\,, \qquad f_z(0,0,0,0)=0\,, \\ &f_x(0,0,0,0)\neq 0\,, \qquad f_{zz}(0,0,0,0)\neq 0\,, \end{aligned} \tag{2}$$

i.e. S is locally given as a graph $x=\varphi(y,z)$. Furthermore the fold-curve L can be locally parameterized by y, i.e. points $p\in L$ are given by $(\xi(y),y,\zeta(y))$, $y\in I$. We project the reduced system

*Work supported by the National Science Foundation under Agreement No. 0112050

onto the (y,z)-plane and obtain

$$\begin{pmatrix} 1 & 0 \\ 0 & -f_z \end{pmatrix} \begin{pmatrix} \dot{y} \\ \dot{z} \end{pmatrix} = \begin{pmatrix} g_2 \\ f_x\, g_1 + f_y\, g_2 \end{pmatrix}\Bigg|_{x=\varphi(y,z)} . \tag{3}$$

Let

$$l(y) := (f_x\, g_1 + f_y\, g_2)|_{p\in L} .$$

We assume

$$l(0) = 0 . \tag{4}$$

From (4) follows that there is a possibility for the reduced flow to cross the fold-curve L with nonzero speed to the repelling branch S_r which is due to a cancellation of a simple zero in the second equation of (3). Such a solution is called a *singular canard.* In correspondence with the phase portrait of the *desingularized* (reduced) system

$$\begin{pmatrix} \dot{y} \\ \dot{z} \end{pmatrix} = \begin{pmatrix} -f_z\, g_2 \\ f_x\, g_1 + f_y\, g_2 \end{pmatrix}\Bigg|_{x=\varphi(y,z)} \tag{5}$$

obtained by multiplying the right hand side of (3) by $-f_z$ (rescaling time), the singularity at the origin is classified as a *folded saddle, folded node, folded degenerate node* or *folded saddle-node (type I/II).* Let $\lambda_{1/2}$ denote the eigenvalues of the linearization at the origin of (5) and let

$$\mu := \frac{\lambda_1}{\lambda_2} . \tag{6}$$

Note that in the folded node case $\mu > 0$ we have a whole sector of singular canards (shadowed region in Figure 1) corresponding to the weak eigendirection (dashed line in Figure 1) of system (5) at the origin. Similarly, a whole sector of singular canards exists in the degenerate folded node

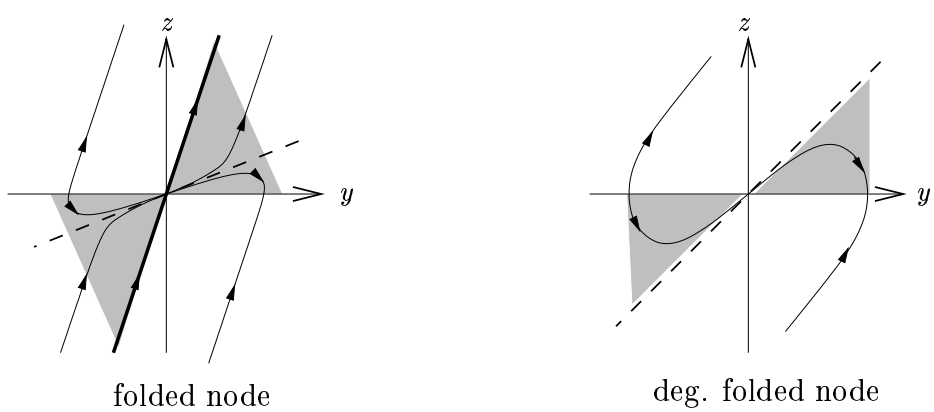

Figure 1: singular canard sectors of reduced flow

case $\mu = 1$. All other singular canards (bold lines in Figure 1 and Figure 2) correspond one-to-one to an eigendirection of (5) at the origin.

The goal is to show persistence of singular canards under small perturbations. The pioneering work on canards in $\mathbb{R}^3$ is due to Benoît [Ben83, Ben90, Ben01]. Based on methods from nonstandard analysis he proved the existence of canard solutions in the folded saddle case. In the folded node

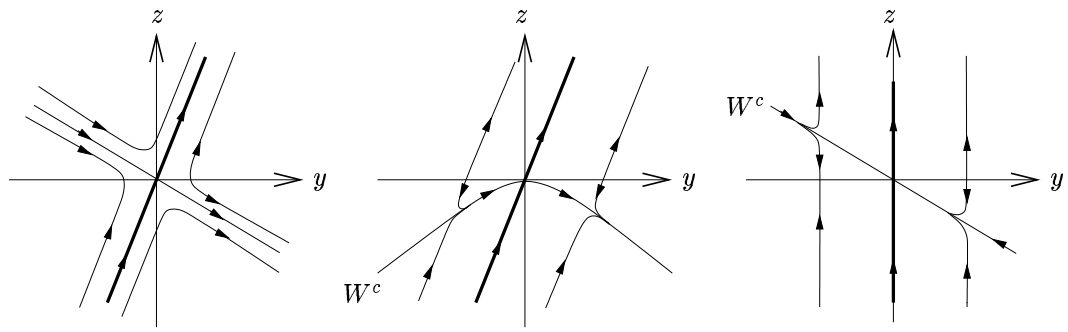

folded saddle folded saddle-node (type I) folded saddle-node (type II)

Figure 2: unique singular canards of reduced flow

case he showed the existence of a pair of *maximal canards* provided the non-resonant condition $\mu \notin \mathbb{N}$ is satisfied. Similar results by means of matched asymptotic expansion can be found in Mishchenko et al. [MKKR94].

We are using geometric singular perturbation theory [Fen79, Jon95] and the blow-up method [DR96, KS99] to show the existence of maximal canards which correspond to intersections of the slow manifolds $S_{a,\varepsilon}$ and $S_{r,\varepsilon}$ of system (1) for $0 < \varepsilon \ll 1$. Szmolyan and Wechselberger [Wec98, SW01] showed that a (unique) singular canard in the folded saddle case and a (unique) singular canard in the folded node case corresponding to the strong eigendirection of system (5) always perturbs to a maximal canard solution of system (1), i.e. the slow manifolds $S_{a,\varepsilon}$ and $S_{r,\varepsilon}$ intersect transversally. Similarly a singular canard in the folded saddle-node (type II) case perturbs to a maximal canard. Note that any solution which is exponentially close to a maximal canard on $S_{a,\varepsilon}$ is a canard solution, i.e. these solutions follow the maximal canard on the repelling branch $S_{r,\varepsilon}$ for a certain amount of time before they get repelled (either back or away).

In this work we focus on the existence and bifurcation of maximal canards corresponding to the sector of singular canards of folded node type. It was shown in [SW01] that a transverse intersection of $S_{a,\varepsilon}$ and $S_{r,\varepsilon}$ exists corresponding to the weak eigendirection (the sector of singular canards) in the folded node case provided that μ is **not** a natural number, i.e. the existence of a (primary) maximal canard. If $n-1 < \mu < n$ then the slow manifolds $S_{a,\varepsilon}$ and $S_{r,\varepsilon}$ twist $n-1$ times around the corresponding maximal canard in the neighbourhood of the fold curve. In the resonant cases, $\mu \in \mathbb{N}$, tranversality is violated and we show that bifurcations of maximal canards occur. This is the mechanism which creates new secondary maximal canards nearby, i.e. other transverse intersections of $S_{a,\varepsilon}$ and $S_{r,\varepsilon}$.

We want to point out that the geometric approach is the right tool to show the bifurcation mechanism of secondary canards from a primary canard. Benoît [Ben90, Ben01] mentioned the existence of secondary canards and gave numerical evidence but did not succeed to prove them. Guckenheimer and Haiduc [GH03] showed numerically secondary canards for large resonances $\mu \gg 1$. Their analysis was based on a perturbation of a folded saddle-node ($\mu \to \infty$). They argued by the rotational properties of the invariant manifolds that the number of secondary canards goes to infinity for $\mu \to \infty$ but without focusing on the underlying bifurcation mechanism.

In Section 2 we make preliminary transformations do bring our system into a canonical form near a folded node singularity. Then we give a detailed geometric analysis using the blow-up technique. Especially we are focusing on the the blown-up reduced flow and its extension onto the blown-up

locus. We restate results given in [SW01] on the existence of the two primary maximal canards for $\mu \notin \mathbb{N}$ and the rotational properties of the invariant manifolds near the maximal canard corresponding to the sector of singular canards.
In Section 3 we focus on the analysis of the resonant cases $\mu \in \mathbb{N}$. We derive bifurcation equations for singular canards by applying an extension of Melnikov-theory given in [Wec02]. Assumptions of this theory are naturally fulfilled in the blow-up analysis by the extensions of center-like manifolds M_a resp. M_r from the entry chart κ_1 into the classical chart κ_2 on the blown-up locus. Thus the bifurcation analysis is naturally carried out in the classical chart κ_2. We show the existence of a transcritical bifurcation of singular canards for odd μ.
In Section 4 we give numerical evidence for the derived transcritical bifurcation for odd μ and for a pitchfork bifurcation for even μ. Furthermore we show that one branch of secondary canards of the transcritical bifurcation and the two branches of secondary canards of the pitchfork bifurcation exist just in a very small neighbourhood U of $\mu \in \mathbb{N}$. The reason is a folding back mechanism of the invariant manifolds on one side of the primary (weak) singular canard due to turning points of the reduced flow nearby. This causes a 'degenerate' bifurcation in the neighbourhood U of the transcritical resp. pitchfork bifurcation and we call this phenomenon a *turning point bifurcation.* Thus the only persistent branch of secondary canards outside U bifurcates from the transcritical bifurcation for $\mu > (2n+1)$, $n \in \mathbb{N}$. We conclude the existence of $[(\mu-1)/2]$ secondary canards for $\mu > 3$ and outside U.
In section 5 we apply our theory to a network of Hodgkin-Huxley (HH) neurons studied in Drover et al [DRSE03]. The network synchronizes rapidly under synaptic excitatory coupling and has a low firing rate of about 10 Hz compared to the intrinsic firing rate of an individual neuron of about 100 Hz. Because of synchrony it suffices to study a single self coupled HH neuron. Standard reduction procedures lead to a HH model with two slow and one fast variables. Studying a FitzHugh-Nagumo model which has the same qualitative features as the HH model shows the existence of canards of folded node type which explains the lowering of the firing rate due to synaptic excitatory coupling.

2 Blow-up analysis

As a starting point for our analysis we show the following

Proposition 2.1 *Assume that system (1) satisfies conditions (2), (4) and that we are in the folded-node scenario. Then there exists a smooth change of time and a smooth change of coordinates which brings system (1) to the form*

$$\begin{aligned} \dot{x} &= \frac{1}{2}\mu y - (\mu+1)z + O(x,\varepsilon,(y+z)^2) \\ \dot{y} &= 1 \\ \varepsilon\dot{z} &= x + z^2 + O(3) + \varepsilon O(1)\,, \end{aligned} \tag{7}$$

in a neighbourhood of the origin where $\lambda_1 = -\mu \in \mathbb{R}^-$ and $\lambda_2 = -1$ correspond to the eigenvalues of the linearization of the desingularized flow of (7).

Proof: A necessary condition to have canards of folded node type is

$$g_2(0,0,0,0) \neq 0\,. \tag{8}$$

Thus we first change time by $d\bar{\tau} = d\tau\, g_2(x,y,z,\varepsilon)$ in (1). Taylor expansion of the functions f, g_1, together with a sequence of linear and near identity transformations gives

$$
(9) \qquad \begin{aligned} \dot{x} &= by + cz + O(x, \varepsilon, (y+z)^2) \\ \dot{y} &= 1 \\ \varepsilon \dot{z} &= x + z^2 + O(3) + \varepsilon O(1)\,, \end{aligned}
$$

with $(b, c) \in \mathbb{R}^2$ computable constants (we omit new coordinate and function notations). In a last step we transform system (9) by

$$
(10) \qquad (x, y, z, t, \varepsilon) \mapsto (\tilde{\lambda}^2 x, \tilde{\lambda}^2 y, -\tilde{\lambda} z, \tilde{\lambda}^2 t, -\tilde{\lambda}^3 \varepsilon),
$$

where $\tilde{\lambda}$ satisfies the characteristic equation $\tilde{\lambda}^2 - \tilde{\lambda} c + 2b = 0$ of the linearization of the desingularized system of (9). With the definition of the parameter

$$
(11) \qquad \mu := \frac{\tilde{\lambda}_1 \tilde{\lambda}_2}{\tilde{\lambda}^2}
$$

we obtain system (7). The corresponding eigenvalues of the linearization of the desingularized system of (7) are $\lambda_1 = -\mu$ and $\lambda_2 = -1$. Thus the notion of the eigenvalue $\lambda_1 = -\mu$ becomes clear by definition (6) of the resonant parameter.

□

Remark: For $\mu \in [1, \infty)$ and $\lambda_1 = -\mu$ and $\lambda_2 = -1$ all resonances of (6) are realized and $\lambda_2 = -1$ corrsponds to the sector of singular canards. We are focusing on this scenario. Of course the same can be realized for $\mu \in (0, 1]$ and $\lambda_1 = -1$ and $\lambda_2 = -\mu$ where again λ_2 corrsponds to the sector of singular canards.

The critical manifold S of (7) is approximately a parabolic cylinder near the origin where the lower branch S_a is attracting while the upper branch S_r is repelling for the corresponding layer problem. The layer problem is the one-dimensional system obtained by changing to the fast time scale $t = \tau/\varepsilon$ in (7) and taking the limit $\varepsilon \to 0$. The fast fibers are simply lines in the z direction.
Fenichel theory [Fen79, Jon95] shows that outside a small neighbourhood U_1 of the fold-curve L the manifolds S_a and S_r perturb smoothly to locally invariant manifolds $S_{a,\varepsilon}$ and $S_{r,\varepsilon}$ for sufficiently small $\varepsilon \neq 0$. Moreover, there exist smooth invariant foliations of the manifold $W^s(S_{a,\varepsilon}) \cap V_1$ in a neighbourhood V_1 of the base $S_{a,\varepsilon}$ and smooth invariant foliations of the manifold $W^u(S_{r,\varepsilon}) \cap V_2$ in a neighbourhood V_2 of the base $S_{r,\varepsilon}$.
Note that the slow manifolds are obtained as sections $\varepsilon = const.$ of three-dimensional, locally invariant, center-like manifolds M_a resp. M_r of the extended (fast) system

$$
(12) \qquad \begin{aligned} x' &= \varepsilon(\frac{1}{2}\mu y - (\mu+1)z + O(x, \varepsilon, (y+z)^2)) \\ y' &= \varepsilon \\ z' &= x + z^2 + O(3) + \varepsilon O(1) \\ \varepsilon' &= 0 \end{aligned}
$$

in the extended phase space $\mathbb{R}^4$. For the extended system $S \times \{0\}$ is a manifold of equilibria. Outside of a neighbourhood U_1 of the fold-curve L the linearization of (12) at points $S_a \times \{0\}$ has a triple zero eigenvalue and one negative eigenvalue uniformly bounded away from zero. This allows to prove the existence of the attracting center-like manifold M_a. The repelling center-like manifold M_r is obtained in a similar way. At the fold-curve the linearization has a quadruple zero

eigenvalue and the construction of the slow manifolds breaks down. Clearly, the slow manifolds can be extended in forward and backward time by the flow, however, their behaviour is then not controlled by the singular limit problems introduced so far.
For that purpose we are using the *blow-up* technique (see e.g. [DR96], [KS99]) to desingularize the flow near nilpotent equilibria like the points on the fold-curve. The blow-up technique is a coordinate transformation by which the degenerate equilibrium at the origin of system (12) is blown-up to a three-sphere. With this procedure one gains enough hyperbolicity to apply standard tools of dynamical systems theory. In our case the blow-up transformation $\Phi : B = S^3 \times \mathbb{R} \to \mathbb{R}^4$ is given by

$$x = r^2\bar{x},\ y = r\bar{y},\ z = r\bar{z},\ \varepsilon = r^2\bar{\varepsilon}\,, \tag{13}$$

with $(\bar{x}, \bar{y}, \bar{z}, \bar{\varepsilon}) \in S^3$. An exposition of the blow-up technique suitable for the analysis of singularly perturbed systems can be found in [SW01]. For the analysis of system (12) it suffices to consider two charts κ_1 and κ_2 defined by $\bar{x} = -1$ resp. $\bar{\varepsilon} = 1$. The singular chart κ_1 gives the extension of the center-like manifolds M_a and M_r onto the blown-up locus. These manifolds are connected on the blown-up locus by special solutions found in the classical chart κ_2. These special solutions can be viewed as extensions of singular canards under consideration.

2.1 Dynamics in chart κ_1

The blow-up $\Phi_1 : \mathbb{R}^4 \to \mathbb{R}^4$ is obtained by setting $\bar{x} = -1$ in (13),

$$\Phi_1(r_1, y_1, z_1, \varepsilon_1) = (-r_1^2, r_1 y_1, r_1 z_1, r_1^2 \varepsilon_1)\,.$$

After transformation of system (12) and desingularization we obtain

$$\begin{aligned} r_1' &= -\frac{1}{2} r_1 \varepsilon_1 g_{11}(r_1, y_1, z_1, \varepsilon_1) \\ y_1' &= \varepsilon_1 (1 + \frac{1}{2} y_1 g_{11}(r_1, y_1, z_1, \varepsilon_1)) \\ z_1' &= -1 + z_1^2 + r_1(\alpha_1 z_1^3 + O(r_1)) + \frac{1}{2}\varepsilon_1 z_1 g_{11}(r_1, y_1, z_1, \varepsilon_1) \\ \varepsilon_1' &= \varepsilon_1^2 g_{11}(r_1, y_1, z_1, \varepsilon_1)\,, \end{aligned} \tag{14}$$

with

$$g_{11}(r_1, y_1, z_1, \varepsilon_1) = \frac{1}{2}\mu y_1 - (\mu + 1) z_1 + O(r_1)\,.$$

There exist two invariant subspaces in system (14), namely the hyperplanes $r_1 = 0$ and $\varepsilon_1 = 0$. In their intersection we find two lines of equilibria $L_{a,1} = (0, y_1, -1, 0)$ and $L_{r,1} = (0, y_1, 1, 0)$ which are normally hyperbolic, the nonzero eigenvalue is -2 for $L_{a,1}$, and 2 for $L_{r,1}$.
Furthermore system (14) has in $\varepsilon_1 = 0$ a normally hyperbolic surface $S_{a,1}$ of equilibria emanating from $L_{a,1}$ and a surface $S_{r,1}$ of equilibria emanating from $L_{r,1}$. Note that $S_{a,1}$ resp. $S_{r,1}$ corresponds to the attracting resp. repelling branch S_a resp. S_r of the critical manifold. We have gained normal hyperbolicity at the lines $L_{a,1}$ and $L_{r,1}$ due to the blow-up (see Figure 3).
In the invariant hyperplane $r_1 = 0$ we recover the lines of equilibria $L_{a,1}$ and $L_{r,1}$ and one additional zero eigenvalue due to the third equation. Hence, there exist a two-dimensional center manifold $C_{a,1}$ resp. $C_{r,1}$ of the line $L_{a,1}$ resp. $L_{r,1}$. This center manifold $C_{a,1}$ resp. $C_{r,1}$ can be viewed as the extension of $S_{a,1}$ resp. $S_{r,1}$ on the blown-up locus. Furthermore there is a time reversing symmetry $\sigma_1(\varepsilon_1, y_1, z_1, t_1) = (\varepsilon_1, -y_1, -z_1, -t_1)$ of system (14) in $r_1 = 0$.

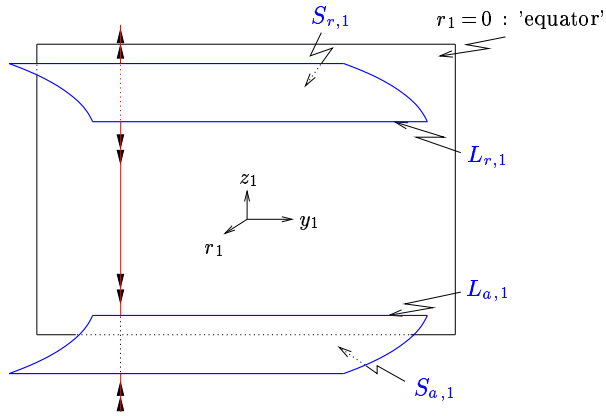

Figure 3: blown-up attracting and repelling manifolds $S_{a,1}$ and $S_{r,1}$ in hyperplane $\varepsilon_1 = 0$

Proposition 2.2 *[SW01] The following holds for system (14):*

1. *There exists an attracting three-dimensional center manifold $M_{a,1}$ of the line of equilibria $L_{a,1}$ containing the surface of equilibria $S_{a,1}$ and the center-manifold $C_{a,1}$. The branch of $C_{a,1}$ in $r_1 = 0$, $\varepsilon_1 \geq 0$ is unique for $y_1 > -2(\mu+1)/\mu$.*

2. *There exists an repelling three-dimensional center manifold $M_{r,1}$ of the line of equilibria $L_{r,1}$ containing the surface of equilibria $S_{r,1}$ and the center-manifold $C_{r,1}$. The branch of $C_{r,1}$ in $r_1 = 0$, $\varepsilon_1 \geq 0$ is unique for $y_1 < 2(\mu+1)/\mu$.*

Note that system (14) corresponds to the blow-up of the fast problem (12). To obtain the corresponding slow flow on the center manifolds $M_{a,1}$ resp. $M_{r,1}$ given by

$$z_1(r_1, \varepsilon_1) = \mp 1 + O(r_1, \varepsilon_1)\,, \tag{15}$$

we plug (15) into system (14) and desingularize:

$$\begin{aligned} r_1' &= -\frac{1}{2} r_1 g_{11}(r_1, y_1, z_1(r_1, \varepsilon_1), \varepsilon_1) \\ y_1' &= 1 + \frac{1}{2} y_1 g_{11}(r_1, y_1, z_1(r_1, \varepsilon_1), \varepsilon_1) \\ \varepsilon_1' &= \varepsilon_1 g_{11}(r_1, y_1, z_1(r_1, \varepsilon_1), \varepsilon_1)\,. \end{aligned} \tag{16}$$

This system has still $\varepsilon_1 = 0$ and $r_1 = 0$ as invariant hyperplanes. The dynamics in $\varepsilon_1 = 0$ represent the (blown-up) reduced flow on $S_{a,1}$ resp. $S_{r,1}$ while the dynamics in $r_1 = 0$ represent the extended flow on $C_{a,1}$ resp. $C_{r,1}$ (on the blown-up sphere).

Lemma 2.1 *System (16) possesses two equilibria $P^-_{\lambda_i}$, $i = 1, 2$ resp. $P^+_{\lambda_i}$, $i = 1, 2$ on $L_{a,1}$ resp. $L_{r,1}$ given by*

$$P^{\pm}_{\lambda_i} = \left(0, \pm\frac{2}{|\lambda_i|}, \pm 1, 0\right)\,, i = 1, 2\,. \tag{17}$$

For $\mu > 1$ these equilibria are saddles. For $\mu = 1$ these equilibria merge and become a saddle-node.

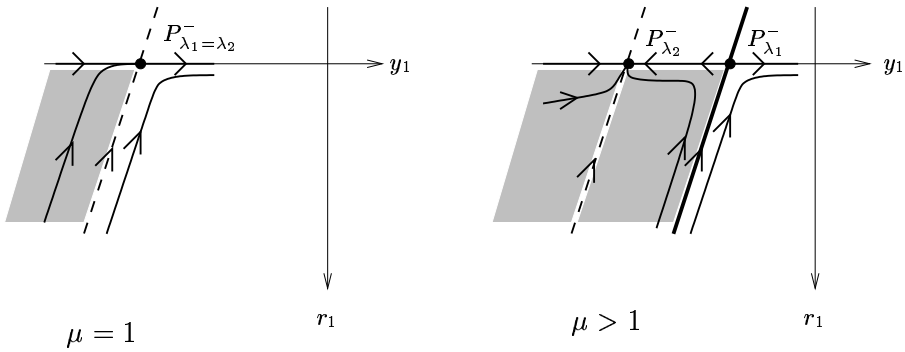

Figure 4: blown-up reduced dynamics on $S_{a,1}$ for $\mu \geq 1$

Note that in the invariant hyperplane $\varepsilon_1 = 0$ the equilibrium $P^\pm_{\lambda_1}$ is a saddle and $P^\pm_{\lambda_2}$ is a node. Thus the (unique) strong eigendirection of the folded node corresponds to the (unique) stable resp. unstable manifold of the saddle $P^-_{\lambda_1}$ resp. $P^+_{\lambda_1}$. The blow-up seperates the strong from the weak eigendirection of the folded node. The projection of the reduced flow on $S_{a,1}$ onto the (y_1, r_1)-plane is shown in Figure 4.
In the invariant hyperplane $r_1 = 0$ the equilibrium $P^\pm_{\lambda_1}$ is a node and $P^\pm_{\lambda_2}$ is a saddle. The projection of the extended flow on $C_{a,1}$ onto the (y_1, ε_1)-plane is illustrated in Figure 5. The dotted line in this figure indicates the ε_1-nullcline given by

$$(y_1, \varepsilon_1) = (-2(\mu + 1)/\mu\,, \varepsilon_1)\,. \tag{18}$$

The flow with respect to ε_1 is increasing for $y_1 > -2(\mu + 1)/\mu$, i.e. in a neighbourhood including the equilibria $P^\pm_{\lambda_1}$ and $P^\pm_{\lambda_2}$. Thus the center manifolds $M_{a,1}$ and $M_{r,1}$ can be extended by the flow

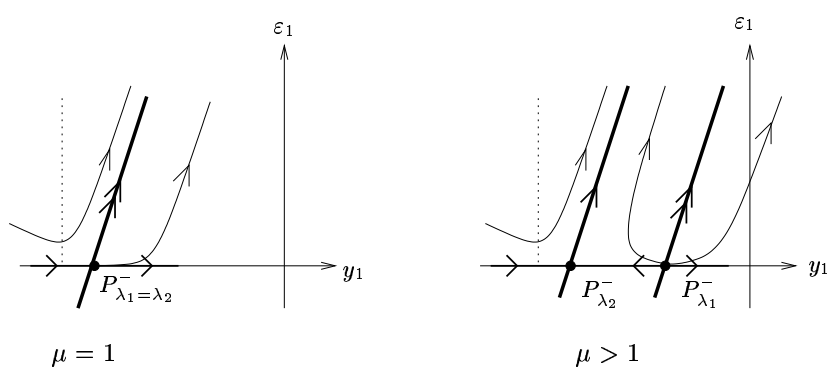

Figure 5: dynamics on $C_{a,1}$ for $\mu \geq 1$, dotted line corresponds to the ε_1-nullcline

onto the blown-up locus near these equilibria. The dynamics on the blown-up locus is covered by the classical chart κ_2. Figure 6 summarizes the invariant dynamics on the center manifold $M_{a,1}$.

2.2 Dynamics in the classical chart κ_2

The blow-up $\Phi_2 : \mathbb{R}^4 \to \mathbb{R}^4$ in chart κ_2 is given by setting $\bar{\varepsilon} = 1$ in (13),

$$\Phi_2(x_2, y_2, z_2, r_2) = (r_2^2 x_2, r_2 y_2, r_2 z_2, r_2^2)\,.$$

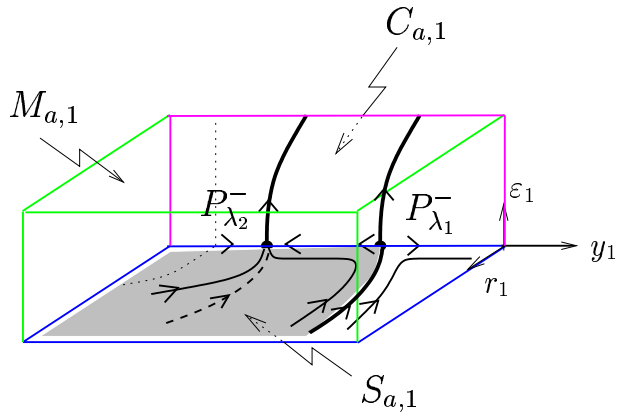

Figure 6: invariant dynamics on $S_{a,1}$ and $C_{a,1}$ within the center manifold $M_{a,1}$

This transformation is just an ε-dependent rescaling of (x, y, z), since $r_2 = \sqrt{\varepsilon}$. After transformation of system (12) and desingularization of the blown-up vector field we obtain

$$\begin{aligned} x_2' &= \frac{1}{2}\mu y_2 - (\mu+1)z_2 + O(r_2) \\ y_2' &= 1 \\ z_2' &= x_2 + z_2^2 + O(r_2)\,. \end{aligned} \tag{19}$$

Setting $r_2 = 0$ gives the unperturbed problem. Two explicit algebraic solutions γ_i, $i = 1, 2$ are known for the unperturbed problem,

$$\gamma_1(t) = (-\frac{\mu^2}{4}t^2 + \frac{\mu}{2}, t, \frac{\mu}{2}t)\,, \tag{20}$$

$$\gamma_2(t) = (-\frac{1}{4}t^2 + \frac{1}{2}, t, \frac{1}{2}t)\,, \tag{21}$$

where γ_1 resp. γ_2 corresponds to the eigenvalue $\lambda_1 = -\mu$ resp. $\lambda_2 = -1$ of the linearization of the desingularized flow. Let κ_{12} denote the change of coordinates from chart κ_2 to chart κ_1:

$$\kappa_{12}(x_2, y_2, z_2, r_2) = \left(r_2\sqrt{-x_2}, \frac{y_2}{\sqrt{-x_2}}, \frac{z_2}{\sqrt{-x_2}}, \frac{1}{-x_2}\right)\,, \qquad x_2 < 0\,. \tag{22}$$

We obtain as limiting behaviour of the special solutions (21) in chart κ_1

$$\lim_{t\to\pm\infty} \kappa_{12}(\gamma_i(t)) = P^{\pm}_{\lambda_i}\,, \quad i = 1, 2\,, \tag{23}$$

where $P^{\pm}_{\lambda_i}$ is given by (17). The importance of the special solutions γ_i, $i=1,2$ is that they connect the attracting manifold across the 'upper half' $\bar{\varepsilon} > 0$ of S^3 to the repelling slow manifold. Thus these special solutions are viewed as extensions of the singular canards in $S_{a,1}$ and $S_{r,1}$. We summarize the properties of the extended system $\{(19), r_2' = 0\}$

Lemma 2.2 *There exist smooth invariant manifolds $M_{a,2}$ and $M_{r,2}$ intersecting along γ_i, $i = 1, 2$. $M_{r,2}$ denotes the extension of the invariant manifold $M_{r,1}$ in backward time, i.e. all solutions of system $\{(19), r_2' = 0\}$ near γ_i, $i = 1, 2$ which are of at most algebraic growth for $t \to \infty$. $M_{r,2}$ denotes the extension of the invariant manifold $M_{r,1}$ in forward time, i.e. all solutions of system $\{(19), r_2' = 0\}$ near γ_i, $i = 1, 2$ which are of at most algebraic growth for $t \to -\infty$.*

Note that $M_{a,2}$ and $M_{r,2}$ are foliated by the parameter r_2. We do our analysis in system (19) and denote the invariant manifolds of system (19) also by $M_{a,2}(r_2)$ and $M_{r,2}(r_2)$ where $M_{a,2}(0) = C_{a,2}$ and $M_{r,2}(0) = C_{r,2}$ are the extensions of the invariant manifolds $C_{a,1}$ and $C_{r,1}$ of Proposition 2.2 in chart κ_2. Furthermore we denote by $M_{a,2}(\gamma_i)$ and $M_{r,2}(\gamma_i)$, $i = 1, 2$ the local invariant manifold $M_{a,2}$ and $M_{r,2}$ near the special solution γ_i, $i = 1, 2$. Studying the intersection of $M_{a,2}(\gamma_1)$ and $M_{r,2}(\gamma_1)$ shows

Proposition 2.3 *[SW01] The slow manifolds $S_{a,\varepsilon}$ and $S_{r,\varepsilon}$ of system (7) intersect transversally along a maximal canard corrsponding to the strong eigendirection of the folded node for $0 < \varepsilon \ll 1$ and for all $\mu > 1$.*

In the following we focus on the intersection of $M_{a,2}(\gamma_2)$ and $M_{r,2}(\gamma_2)$. The goal is to describe all possible solutions of (19) near γ_2 which are of at most algebraic growth for $t \to \pm\infty$. To get a better geometrical understanding for our analysis we first rectify γ_2 along the z_2-axis. This is done by a coordinate transformation $(x_2, y_2, z_2) \mapsto (x_2 + z_2^2 - 1/2, y_2 - 2z_2, 2z_2)$ which brings system (19) to

$$\begin{aligned} x_2' &= \frac{1}{2}\mu y_2 + x_2 z_2 + O(r_2) \\ y_2' &= -2x_2 + O(r_2) \\ z_2' &= 2x_2 + 1 + O(r_2)\,, \end{aligned} \tag{24}$$

where we have omitted new coordinate notations. The parameter μ is the same as in system (19). The special solution γ_2 is transformed to

$$\gamma_2(t) = (0, 0, t),\ t \in \mathbb{R}. \tag{25}$$

Next we transform system (24) along γ_2 which gives the non-autonomous system

$$v' = A(t, \mu_0)v + g(t, v, \mu, r_2) \tag{26}$$

with $v = (v_1, v_2, v_3)$, linear part

$$A(t, \mu_0) = \begin{pmatrix} t & \frac{1}{2}\mu_0 & 0 \\ -2 & 0 & 0 \\ 2 & 0 & 0 \end{pmatrix}. \tag{27}$$

and

$$g(t, v, \mu, r_2) = f(\gamma(t) + v, \mu, r_2) - f(\gamma(t), \mu_0, 0) - A(t, \mu_0)v \tag{28}$$

where f denotes the right hand side of (24). We denote by $\Phi(t, s)$, $t, s \in \mathbb{R}$, the transition matrix of the variational equation along γ_2:

$$v' = A(t, \mu_0)v\,. \tag{29}$$

The variational equation can be written as a second order homogeneous equation

$$v_1'' - tv_1' + (\mu_0 - 1)v_1 = 0 \tag{30}$$

which is called the *Weber equation*. If $\mu_0 \in \mathbb{N}$ then the *Hermite polynomial* $H_{\mu_0-1}(t/\sqrt{2})$ is a solution of (30) of algebraic growth. If $\mu_0 \notin \mathbb{N}$ then all solutions of (30) grow exponentially either in forward or backward time. Thus $\mu_0 \notin \mathbb{N}$ is a sufficient condition to prove transversal intersection of the invariant manifolds $C_{a,2}(\gamma_2)$ and $C_{r,2}(\gamma_2)$ in $r_2 = 0$. It follows

Proposition 2.4 *[SW01] Given system (7) and $1 < \mu \notin \mathbb{N}$. Then the slow manifolds $S_{a,\varepsilon}$ and $S_{r,\varepsilon}$ intersect transversally along a (primary) maximal canard for $0 < \varepsilon \ll 1$ corresponding to the sector of singular canards.*

We introduce an affine coordinate $w = v_1/v_2$ in the variational equation (29). This coordinate measures the rotation (in the projective space) of the tangent bundles of $C_{a,2}(\gamma_2)$ and $C_{r,2}(\gamma_2)$ along $\dot{\gamma}_2$ and gives a Riccati equation

$$w' - 2w^2 - tw - \mu_0/2 = 0\,. \tag{31}$$

With the substitution $w = -u'/2u$ this Riccati equation is transformed into a second order linear equation and we obtain again a Weber equation

$$u'' - tu' + \mu_0 u = 0\,. \tag{32}$$

Proposition 2.5 *[SW01] Given system (7) and $n-1 < \mu < n$. Then the invariant manifolds $S_{a,\varepsilon}$ and $S_{r,\varepsilon}$ twist $(n-1/2)\pi$ times around the (primary) maximal canard of Proposition 2.4.*

At a resonance $\mu_0 \in \mathbb{N}$ the tangent bundles match up forming a single band with n twists. In these resonant cases $\mu_0 \in \mathbb{N}$ we have a two-dimensional contact of the invariant manifolds $C_{a,2}(\gamma_2)$ and $C_{r,2}(\gamma_2)$ and bifurcation of secondary canards is expected. We will apply an extension of Melnikov-theory for invariant manifolds on noncompact domains developed in [Wec02] to analyse these resonances.

3 Melnikov analysis

The variational equation (29) possesses dichotomy properties, i.e. there exist continous projection maps P_+ resp. Q_- such that

$$\begin{aligned} \mathcal{R}(P_+(t)) &= T_{\gamma_2(t)}C_{r,2}(\gamma_2), \qquad t \geq 0 \\ \mathcal{R}(Q_-(t)) &= T_{\gamma_2(t)}C_{a,2}(\gamma_2), \qquad t \leq 0\,. \end{aligned}$$

Hence we call $\mathcal{R}(P_+(t))$ the center-subspace of (29) at $t \geq 0$ and $\mathcal{R}(Q_-(t))$ the center-subspace of (29) at $t \leq 0$. Let the phase-space $\mathbb{R}^3$ split as follows:

$$\mathbb{R}^3 = span\{\dot{\gamma}_2(0)\} \oplus U \oplus \mathcal{W}\,, \tag{33}$$

with $\|\dot{\gamma}_2(0)\| = 1$ where

$$\begin{aligned} span\{\dot{\gamma}_2(0)\} \oplus U &= T_{\gamma_2(0)}C_{r,2}(\gamma_2) \cap T_{\gamma_2(0)}C_{a,2}(\gamma_2) \\ \mathcal{W} &= (T_{\gamma_2(0)}C_{r,2}(\gamma_2) + T_{\gamma_2(0)}C_{a,2}(\gamma_2))^{\perp}\,. \end{aligned}$$

Note that $\mathcal{W}$ denotes the subspace of all bounded solution of the adjoint equation of (29)

$$\psi' + A(t,\mu_0)^T\psi = 0\,, \tag{34}$$

which decays exponentially in forward and backward time. Next we define Banach-spaces suitable for our problem:

$$C_b^0(\mathbb{R}_+,\mathbb{R}^3) := \{v \in C^0(\mathbb{R}_+,\mathbb{R}^3) |\ \|v\|_+ := \sup_{t\geq 0}\{\|v(t)\| \cdot t^{-\delta}\} < \infty\}\,, \tag{35}$$

$$C_b^0(\mathbb{R}_-,\mathbb{R}^3) := \{v \in C^0(\mathbb{R}_-,\mathbb{R}^3) |\ \|v\|_- := \sup_{t\leq 0}\{\|v(t)\| \cdot |t|^{-\delta}\} < \infty\}\,, \tag{36}$$

with $\delta \in \mathbb{N}$ sufficiently large. Thus, solutions of (26) which are in these Banach-spaces determine the center-manifolds $M_{r,2}(r_2)$ resp. $M_{a,2}(r_2)$. Using the variation of constant formula for solutions of (26) it follows that $v \in C_b^0(\mathbb{R}_+, \mathbb{R}^3)$ resp. $v \in C_b^0(\mathbb{R}_-, \mathbb{R}^3)$ is a solution of (26) if and only if there exists a vector $\xi \in \mathcal{R}(P_+(0)) = \mathcal{R}(Q_-(0))$ such that

$$v_+(t) = \Phi(t,0)\xi + \int_0^t \Phi(t,s)P_+(s)g(s,v_+,\mu,r_2)\,ds + \int_\infty^t \Phi(t,s)Q_+(s)g(s,v_+,\mu,r_2)\,ds \tag{37}$$

for $t \in \mathbb{R}_+$ and $Q_+ = I - P_+$ resp.

$$v_-(t) = \Phi(t,0)\xi + \int_0^t \Phi(t,s)Q_-(s)g(s,v_-,\mu,r_2)\,ds + \int_{-\infty}^t \Phi(t,s)P_-(s)g(s,v_-,\mu,r_2)\,ds \tag{38}$$

for $t \in \mathbb{R}_-$ and $P_- = I - Q_-$. It follows by the implicit function theorem in Banach-spaces that $v_+ = v_+(\rho,\mu,r_2)$ resp. $v_- = v_-(\rho,\mu,r_2)$ near the origin. Let ρ be the coordinate in the subspace U and $D = D(\rho,\mu,r_2)$ denote a distance-function which measures the distance between solutions v_- and v_+ in a transversal section to the special solution γ_2 at $t=0$, i.e. in the subspace $U \oplus \mathcal{W}$. Then $D(\rho,\mu,r_2) = 0$ denotes the bifurcation equation for solutions of (26) which are of at most algebraic growth for $t \to \pm\infty$.

Proposition 3.1 *[Wec02] An analytic expression for the distance function D is given by*

$$D(\rho,\mu,r_2) := \int_{-\infty}^{\infty} \langle \psi(s), g(s, v(\rho,\mu,r_2)(s),\mu,r_2)\rangle\,ds\,, \tag{39}$$

where $\psi(s)$ is a bounded solution of the adjoint equation (34) which decay exponentially in forward and backward time.

Usually the bifurcation equation $D(\rho,\mu,r_2) = 0$ cannot be solved explicitly. Thus one tries to analyse the equation in the neighbourhood of $(0,\mu_0,0)$, $\mu_0 \in \mathbb{N}$ with the implicit function theorem or more generally by means of singularity theory (Arnold [Arn81], Golubitsky, Schaeffer [GS84]). For this purpose we Taylor expand the distance function

$$D(\rho,\mu,r_2) = \frac{\partial D}{\partial \rho}(0,\mu_0,0)\rho + \frac{\partial D}{\partial \mu}(0,\mu_0,0)\,(\mu-\mu_0) + \frac{\partial D}{\partial r_2}(0,\mu_0,0)\,r_2 + h.o.t.\,, \tag{40}$$

where the partial derivatives of the distance function (39) at $(\rho,\mu,r_2) = (0,\mu_0,0)$ are called *Melnikov-integrals (Melnikov-functions)*. We state our main result

Theorem 3.1 *For odd μ_0 exists a transcritical bifurcation of singular canards near γ_2 in the unperturbed system of (19), i.e. the bifurcation equation $D(\rho,\mu,0) = 0$ is locally equivalent to the normal form*

$$\rho^2 + (-1)^{\frac{\mu_0+1}{2}}\rho(\mu-\mu_0) = 0\,, \qquad \mu_0 = odd\,. \tag{41}$$

The proof is given in the following by calculating the Melnikov-integrals up to second order. For the calculation of the Melnikov-integrals we need an explicit bounded solution ψ of the adjoint equation (34) which decays exponentially for $t \to \pm\infty$. The adjoint equation (34) can be written as a homogeneous second order differential equation

$$\psi_1'' + t\psi_1' + (\mu_0+1)\psi_1 = 0\,. \tag{42}$$

The transformation $\psi_1(t) = \varphi(t)\exp(-t^2/2)$ brings (42) to the Weber-equation

$$\varphi'' - t\varphi' + \mu_0\varphi = 0\,, \tag{43}$$

where one solution is given by the Hermite-polynomial $H_{\mu_0}(t/\sqrt{2})$ for $\mu_0 \in \mathbb{N}$. Thus, the solution ψ which decays exponentially for $t \to \pm\infty$ is given by

$$\begin{pmatrix} \psi_1(t) \\ \psi_2(t) \\ \psi_3(t) \end{pmatrix} = k_1 \begin{pmatrix} H_{\mu_0}(t/\sqrt{2}) \\ \mu_0 H_{\mu_0-1}(t/\sqrt{2})/\sqrt{2} \\ 0 \end{pmatrix} \exp(\frac{-t^2}{2}), \qquad \mu_0 \in \mathbb{N}, \tag{44}$$

where

$$k_1 = \begin{cases} \frac{\sqrt{2}}{\mu H_{\mu_0-1}(0)} & \mu_0 = \text{odd} \\ \\ \frac{1}{H_{\mu_0}(0)} & \mu_0 = \text{even} \end{cases} \tag{45}$$

such that $\|\psi(0)\| = 1$. Recall, that $\psi(0) \in \mathcal{W}$. Similar follows from (30) and $\mu_0 \in \mathbb{N}$ that the transition matrix of the variational equation is of the form

$$\Phi(t,0) = \begin{pmatrix} H_{\mu_0-1}(t/\sqrt{2})/H_{\mu_0-1}(0) & * & 0 \\ -\sqrt{2}H_{\mu_0}(t/\sqrt{2})/(\mu_0 H_{\mu_0-1}(0)) & * & 0 \\ \sqrt{2}H_{\mu_0}(t/\sqrt{2})/(\mu_0 H_{\mu_0-1}(0)) & * & 1 \end{pmatrix} \qquad \mu_0 = \text{odd} \tag{46}$$

$$\Phi(t,0) = \begin{pmatrix} * & -\mu_0 H_{\mu_0-1}(t/\sqrt{2})/(\sqrt{2}H_{\mu_0}(0)) & 0 \\ * & H_{\mu_0}(t/\sqrt{2})/H_{\mu_0}(0) & 0 \\ * & -H_{\mu_0}(t/\sqrt{2})/H_{\mu_0}(0) + 1 & 1 \end{pmatrix} \qquad \mu_0 = \text{even} \tag{47}$$

where $H_0(0) = 1$ and $H_n(0) = (-2)^{n/2}(n-1)!$ for even n (the asterisks denote an unspecified column of the transition matrix). The splitting of the phase space (33) for our Melnikov-calculations is given by

$$\mathbb{R}^3 = span\left\{\begin{pmatrix} 0 \\ 0 \\ 1 \end{pmatrix}\right\} \oplus span\left\{\begin{pmatrix} 1 \\ 0 \\ 0 \end{pmatrix}\right\} \oplus span\left\{\begin{pmatrix} 0 \\ 1 \\ 0 \end{pmatrix}\right\}, \qquad \mu_0 = \text{odd}, \tag{48}$$

$$\mathbb{R}^3 = span\left\{\begin{pmatrix} 0 \\ 0 \\ 1 \end{pmatrix}\right\} \oplus span\left\{\begin{pmatrix} 0 \\ 1 \\ 0 \end{pmatrix}\right\} \oplus span\left\{\begin{pmatrix} 1 \\ 0 \\ 0 \end{pmatrix}\right\}, \qquad \mu_0 = \text{even}. \tag{49}$$

Lemma 3.1

$$\frac{\partial D}{\partial \rho}(0, \mu_0, 0) = 0 \tag{50}$$

Proof: By definition of the function $g(t, v, \mu, r_2)$ (28) we have $g(t, 0, \mu_0, 0) = 0$ and

$$\frac{\partial g}{\partial v}(t, 0, \mu_0, 0) = \frac{\partial f}{\partial x}(\gamma_2(t), \mu_0, 0) - A(t, \mu_0) = 0 \tag{51}$$

where $x = (x_2, y_2, z_2) \in \mathbb{R}^3$. Hence, it follows immediately that

$$\frac{\partial D}{\partial \rho}(0, \mu_0, 0) = \int_{-\infty}^{\infty} \langle \psi(s), \frac{\partial g}{\partial v}(s, 0, \mu_0, 0) \frac{\partial v}{\partial \rho}(0, \mu_0, 0)(s) \rangle \, ds = 0$$

□

This result keeps the fact that generically the bifurcation equation cannot be solved for ρ by the implicit function theorem and that a bifurcation of canards occurs.

Lemma 3.2

$$\frac{\partial D}{\partial \mu}(0,\mu_0,0) = 0 \tag{52}$$

Proof: The Melnikov-integral is given by

$$\frac{\partial D}{\partial \mu}(0,\mu_0,0) = \int_{-\infty}^{\infty} \langle \psi(s), \frac{\partial f}{\partial \mu}(\gamma_2(s),\mu_0,0)\rangle \, ds \, .$$

The result follows immediately from

$$\frac{\partial f}{\partial \mu}(\gamma_2(s),\mu_0,0) = 0 \tag{53}$$

□

Lemma 3.3

$$\frac{\partial^2 D}{\partial \mu^2}(0,\mu_0,0) = 0 \tag{54}$$

Proof:

$$\begin{aligned} \frac{\partial^2 D}{\partial \mu^2}(0,\mu_0,0) \;=\; & \int_{-\infty}^{\infty} \langle \psi(s), \frac{\partial^2 f}{\partial x^2}(\gamma_2(s),\mu_0,0) \left(\frac{\partial v}{\partial \mu}(0,\mu_0,0)(s), \frac{\partial v}{\partial \mu}(0,\mu_0,0)(s) \right) \rangle \, ds \, + \\ & \int_{-\infty}^{\infty} \langle \psi(s), \frac{\partial^2 f}{\partial x \partial \mu}(\gamma_2(s),\mu_0,0) \frac{\partial v}{\partial \mu}(0,\mu_0,0)(s) + \frac{\partial^2 f}{\partial \mu^2}(\gamma_2(s),\mu_0,0)\rangle \, ds \, . \end{aligned} \tag{55}$$

The result follows from

$$\left(\frac{\partial f}{\partial \mu}(\gamma_2(s),\mu_0,0) = 0 \, , \frac{\partial g}{\partial v}(t,0,\mu_0,0) = 0 \right) \;\Rightarrow\; \frac{\partial v}{\partial \mu}(0,\mu_0,0)(s) = 0 \tag{56}$$

and

$$\frac{\partial^2 f}{\partial \mu^2}(\gamma_2(s),\mu_0,0) = 0 \tag{57}$$

□

Proposition 3.2

$$\frac{\partial^2 D}{\partial \rho^2}(0,\mu_0,0) = \begin{cases} \delta_{\rho\rho} \neq 0 & \mu_0 = \; odd \\ 0 & \mu_0 = \; even \end{cases} \tag{58}$$

Proof:

$$\frac{\partial^2 D}{\partial \rho^2}(0,\mu_0,0) = \int_{-\infty}^{\infty} \langle \psi(s), \frac{\partial^2 f}{\partial x^2}(\gamma_2(s),\mu_0,0) \left(\frac{\partial v}{\partial \rho}(0,\mu_0,0)(s), \frac{\partial v}{\partial \rho}(0,\mu_0,0)(s) \right) \rangle \, ds \tag{59}$$

From the definition of (37) resp. (38) it follows that

$$\frac{\partial v}{\partial \rho}(0,\mu_0,0)(s) = \Phi(s,0) \frac{\partial \xi}{\partial \rho} \, .$$

As the measuring of distance-function D just takes place in transverse directions of $\gamma_2(0)$ we set $\xi = \xi(\rho) = \rho u \in U$. Thus

$$\frac{\partial v_\pm}{\partial \rho}(0,\mu_0,0)(s) = \Phi(s,0)u$$

is a solution of at most algebraic growth of the variational equation (29). With the splitting of our phase space (48) and definition of the transition matrix (46) (resp. (49) and (47)) we obtain

$$\frac{\partial v}{\partial \rho}(0,\mu_0,0)(s) = \begin{pmatrix} H_{\mu_0-1}(t/\sqrt{2})/H_{\mu_0-1}(0) \\ -\sqrt{2}H_{\mu_0}(t/\sqrt{2})/(\mu_0 H_{\mu_0-1}(0)) \\ \sqrt{2}H_{\mu_0}(t/\sqrt{2})/(\mu_0 H_{\mu_0-1}(0)) \end{pmatrix} \quad \mu_0 = \text{odd} \tag{60}$$

$$\frac{\partial v}{\partial \rho}(0,\mu_0,0)(s) = \begin{pmatrix} -\mu_0 H_{\mu_0-1}(t/\sqrt{2})/(\sqrt{2}H_{\mu_0}(0)) \\ H_{\mu_0}(t/\sqrt{2})/H_{\mu_0}(0) \\ -H_{\mu_0}(t/\sqrt{2})/H_{\mu_0}(0)+1 \end{pmatrix} \quad \mu_0 = \text{even} \tag{61}$$

Using this result and definition (44) in (59) we get for even μ_0

$$\begin{aligned} \frac{\partial^2 D}{\partial \rho^2}(0,\mu_0,0) &= \frac{\sqrt{2}\mu_0}{H^3_{\mu_0}(0)} \int_{-\infty}^{\infty} H_{\mu_0}(s/\sqrt{2})^2 H_{\mu_0-1}(s/\sqrt{2}) \exp\left(\frac{-s^2}{2}\right) ds \\ &= 0\,, \end{aligned}$$

resp. for odd μ_0

$$\begin{aligned} \frac{\partial^2 D}{\partial \rho^2}(0,\mu_0,0) &= \frac{4}{\mu_0^2 H^3_{\mu_0-1}(0)} \int_{-\infty}^{\infty} H_{\mu_0}(s/\sqrt{2})^2 H_{\mu_0-1}(s/\sqrt{2}) \exp\left(\frac{-s^2}{2}\right) ds \\ &= \frac{4}{\mu_0^2 H^3_{\mu_0-1}(0)} \frac{2^{\frac{3\mu_0+1}{2}}(\mu_0!)^3}{(\frac{\mu_0-1}{2}!)^3 \mu_0(\mu_0+1)} \sqrt{2\pi} =: \delta_{\rho\rho}\,, \end{aligned}$$

which gives the assertion.

□

Proposition 3.3

$$\frac{\partial^2 D}{\partial \rho \partial \mu}(0,\mu_0,0) = \delta_{\rho\mu} \neq 0 \qquad \mu_0 \in \mathbb{N} \tag{62}$$

Proof:

$$\begin{aligned} \frac{\partial^2 D}{\partial \rho \partial \mu}(0,\mu_0,0) &= \int_{-\infty}^{\infty} \langle \psi(s), \frac{\partial^2 f}{\partial x^2}(\gamma_2(s),\mu_0,0) \left(\frac{\partial v}{\partial \mu}(0,\mu_0,0)(s), \frac{\partial v}{\partial \rho}(0,\mu_0,0)(s)\right)\rangle\, ds + \\ &\quad \int_{-\infty}^{\infty} \langle \psi(s), \frac{\partial^2 f}{\partial x \partial \mu}(\gamma_2(s),\mu_0,0) \frac{\partial v}{\partial \rho}(0,\mu_0,0)(s)\rangle\, ds\,. \end{aligned} \tag{63}$$

Recall that $\xi = \xi(\rho)$. Thus it follows from definition (37) resp. (38) and (53) that

$$\frac{\partial v}{\partial \mu}(0,\mu_0,0)(s) = \Phi(s,0)\frac{\partial \xi}{\partial \mu} = 0\,. \tag{64}$$

Using this result and definitions (44) and (60) resp. (61) in (63) we obtain for $\mu_0 \in \mathbb{N}$

$$\begin{aligned} \frac{\partial^2 D}{\partial \rho \partial \mu}(0,\mu_0,0) &= k_2 \int_{-\infty}^{\infty} H(\mu_0, s/\sqrt{2})^2 \exp\left(\frac{-s^2}{2}\right) ds \\ &= k_2\, 2^{\mu_0} \mu_0! \sqrt{2\pi} =: \delta_{\rho\mu}\,, \end{aligned}$$

where

$$k_2 = \begin{cases} -(\mu_0 H_{\mu_0-1}(0))^{-2} & \mu_0 = \text{odd} \\ (2H^2_{\mu_0}(0))^{-1} & \mu_0 = \text{even} \end{cases} \tag{65}$$

□

Singularity theory [GS84] gives then the equivalence of $D(\rho, \mu, 0) = 0$ with the normal form (41) which is called the recognition problem. The assertion of Theorem 3.1 follows. Note that in the case $\mu = 1$ of the degenerate folded node we have a transcritical bifurcation given by the two special solutions γ_i, $i = 1, 2$ which we call the primary singular canards. All other bifurcating singular canards we call secondary.

Remark: To state a similar result for even μ_0 (most likely a pitchfork bifurcation) we would need results on third order Melnikov-integrals but these cannot be solved analytically.

4 Numerical analysis

We state the following result on the existence of secondary canards.

Proposition 4.1 *Let $I = (3, \infty)$, U be the union of neighbourhoods of the resonances $\mu_o \in \mathbb{N}$ and $\mu \in I/U$. Then system (7) possesses $[(\mu - 1)/2]$ secondary maximal canards.*

Remember that $M_{a,2}(0) = C_{a,2}$ resp. $M_{r,2}(0) = C_{r,2}$ are the extensions of the invariant manifolds $C_{a,1}$ resp. $C_{r,1}$ in chart κ_2 and that singular canards are intersections of $C_{a,2}$ and $C_{r,2}$. A crucial observation of Proposition 2.2 is that $C_{a,1}$ resp. $C_{r,1}$ is unique for $y_1 > -2(\mu + 1)/\mu$ resp. $y_1 < 2(\mu + 1)/\mu$ because the flow is directed away from resp. towards the line of equilibria $L_{a,1}$ resp. $L_{r,1}$ (saddle property). We fix a curve $\varepsilon_1 = \delta$ of initial conditions in $C_{a,1}$ (resp. $C_{r,1}$) (see Figure 7). Then there exists a tangency for the flow and the curve of initial conditions at the intersection

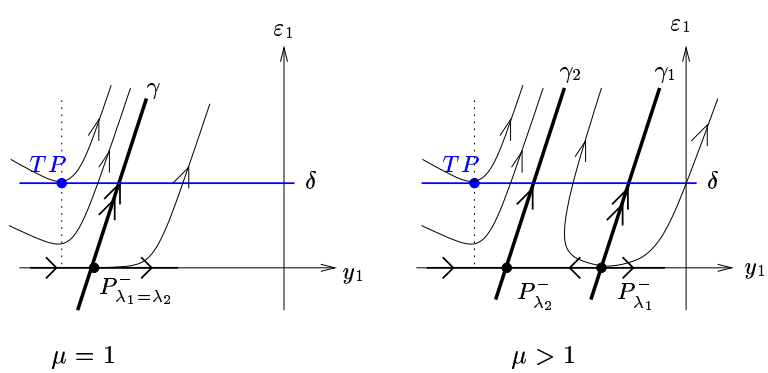

Figure 7: line of initial conditions on $C_{a,1}$ (blue) and turning point (TP) of the flow, dotted line is ε_1-nullcline

with the ε_1 nullcline (18). We call this point a turning point which is given by

$$TP_{a/r,1}(y_1, z_1, \varepsilon_1) = (\mp 2(\mu + 1)/\mu\,, \mp 1, \delta)\,. \tag{66}$$

All trajectories with initial conditions left of the turning point on $C_{a,1}$, i.e. $y_1 < -2(\mu + 1)/\mu$, are folded by the flow onto the trajectories with initial conditions between the turning point and the

special solution γ_2. By the time reversing symmetry σ_1 the same holds on $C_{r,1}$. In the following we integrate initial conditions between the turning point and the ε_1 axis to obtain a sufficiently global picture of the extension of the manifolds $C_{a,1}$ and $C_{r,1}$ in a neighbourhood of the primary canards $\gamma_{1/2}$. This segment of initial conditions is given by

$$IC_{a/r,1}(y_1, z_1, \varepsilon_1) = (\pm y_1, \mp 1 + O(\delta), \delta)\,. \tag{67}$$

with $-2(\mu+1)/\mu \leq y_1 < 0$. The numerical calculations are done in chart κ_2 for the unperturbed system

$$\begin{aligned} x_2' &= \frac{1}{2}\mu y_2 - (\mu+1)z_2 \\ y_2' &= 1 \\ z_2' &= x_2 + z_2^2 \end{aligned} \tag{68}$$

to show intersections of the invariant manifolds $C_{a,2}$ and $C_{r,2}$. Applying the change of coordinates (22) we obtain the segment of initial condiations in chart κ_2

$$IC_{a/r,2}(x_2, y_2, z_2) = (-1/\delta, \pm y_2, \sqrt{1/\delta}(\mp 1 + O(\delta)) \tag{69}$$

with $-2\sqrt{1/\delta}(\mu+1)/\mu \leq y_2 < 0$. The turning point (66) is given in chart κ_2 by

$$TP_{a/r,2}(x_2, y_2, z_2) = (-1/\delta, \pm\sqrt{1/\delta}(\mu+1)/\mu, \mp\sqrt{1/\delta})\,. \tag{70}$$

We integrate the trajectories with initial conditions on $IC_{a,2}$ in forward time until the intersect the plane $y_2 = 0$ which is a transverse section for the flow. System (68) possesses the time reversing symmetry $\sigma_2(x_2, y_2, z_2, t_2) = (x_2, -y_2, -z_2, -t_2)$ which recovers the time reversing symmetry σ_1 in chart κ_1. Thus by applying this symmetry to $(y_2 = 0) \cap C_{a,2}$ gives exactly the intersection $(y_2 = 0) \cap C_{r,2}$ with initial conditions on $IC_{r,2}$ and integrated in backward time. Obviously, singular canards are intersection points of $(y_2 = 0) \cap (C_{r,2} \cap C_{a,2})$. Note that the primary canards (21) are given by

$$\begin{aligned} (z_2 = 0) \cap \gamma_1 &= (\mu/2, 0) \\ (z_2 = 0) \cap \gamma_2 &= (1/2, 0) \end{aligned} \tag{71}$$

We fix $\delta = 1/100$ in (69) for all our numerical integrations. Figure 8 shows the intersections of $C_{r,2}$ (blue) and $C_{a,2}$ (red) for several values of μ. We observe the tangencies of the invariant manifolds $C_{r,2}$ and $C_{a,2}$ at γ_2 for $\mu \in \mathbb{N}$ as well as the transverse intersection for $\mu \notin \mathbb{N}$ stated in Proposition 2.4. Note the bifurcating primary (strong) canard γ_1 with its robust transverse intersection of $C_{r,2}$ and $C_{a,2}$ stated in Proposition 2.3. Furthermore a secondary canard has bifurcated from γ_2 for $\mu \geq 3$.

Figure 9 shows zooms in the neighbourhood of γ_2 near the transcritical bifurcation at $\mu = 3$. Note the short branches of the invariant manifolds. The tip of each branch is the image of the trajectory with the turning point $TP_{a/r,2}$ as initial condition. The manifold $C_{r,2}$ resp. $C_{a,2}$ does not end at the tip but get folded back onto the branch between the tip and the primary canard γ_2. Because of that we observe another bifurcation of secondary canards at $\mu \approx 2.995$. We call this bifurcation a *turning point bifurcation* (TPB).

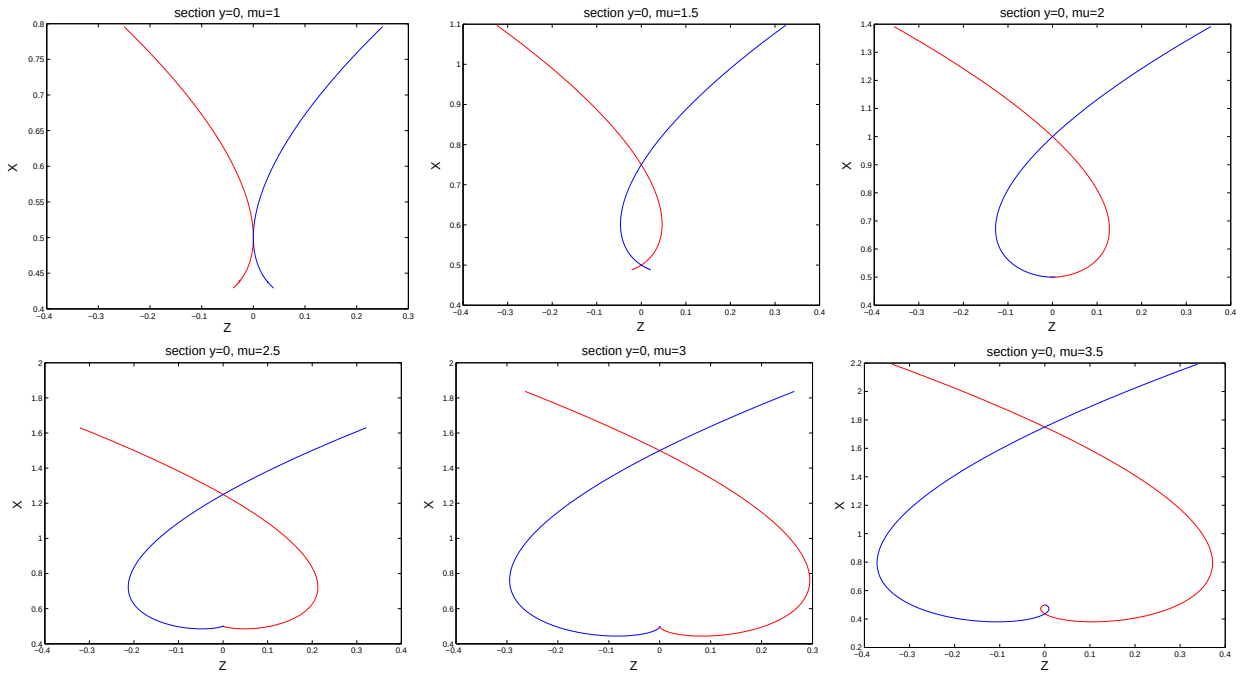

Figure 8: intersection of manifolds $C_{r,2}$ (blue) and $C_{a,2}$ (red) in $y_2 = 0$

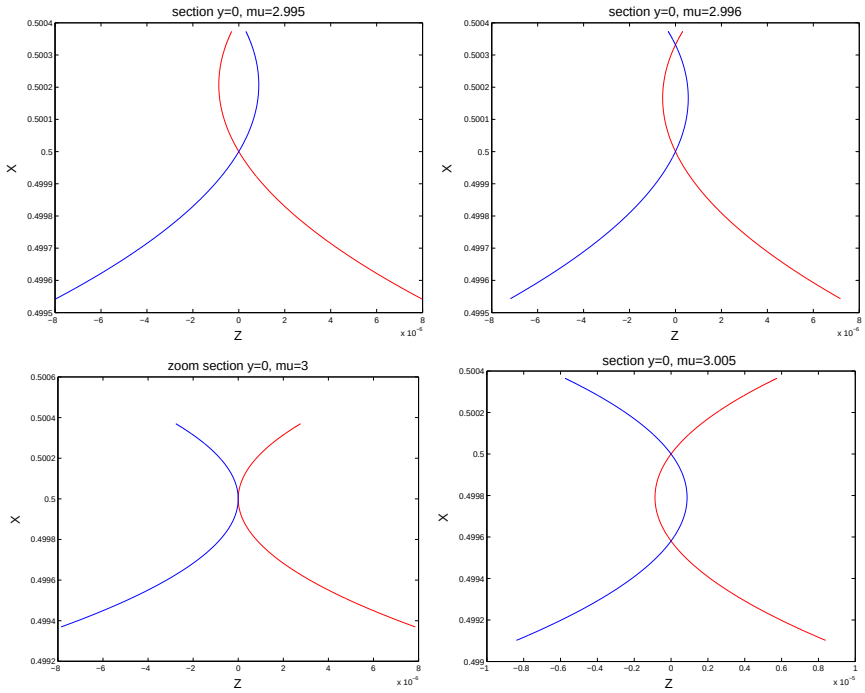

Figure 9: intersection of manifolds $C_{r,2}$ (blue) and $C_{a,2}$ (red) in $y_2 = 0$ near a transcritical (TC) bifurcation at $\mu = 3$; furthermore a turning point bifurcation (TPB) is observed at $\mu \approx 2.995$

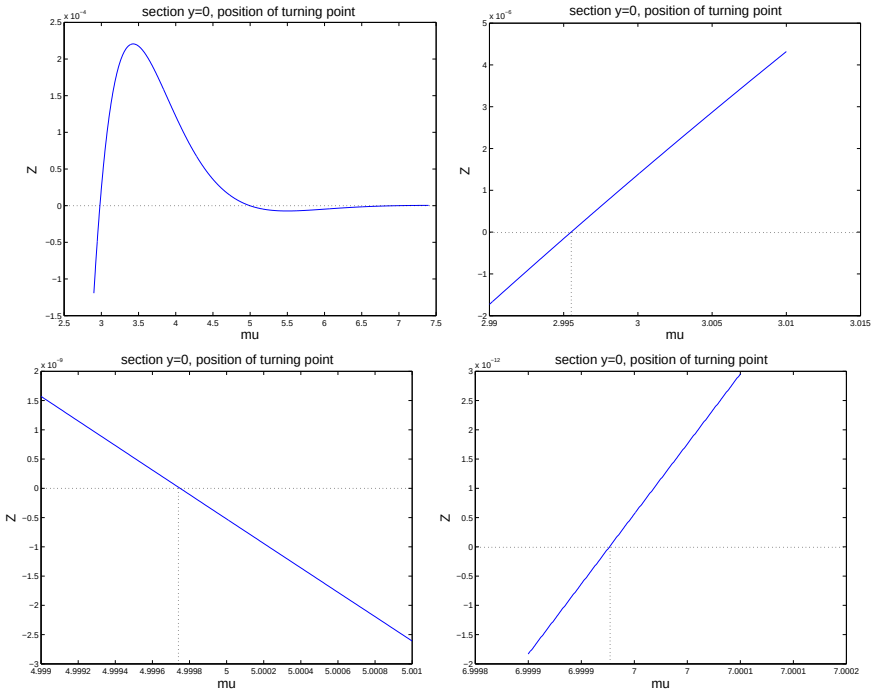

Figure 10: position of turning point (TP) in $y_2 = 0$ as a function of μ; turning point bifurcations (TPB) are observed at $\mu \approx 2.995$, $\mu \approx 4.9998$ and $\mu \approx 6.99995$

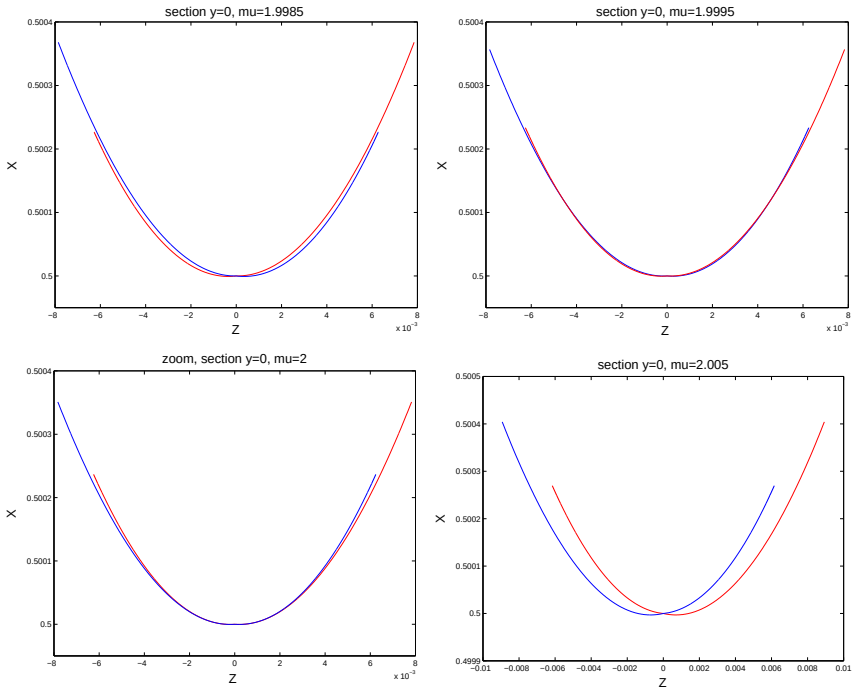

Figure 11: intersection of manifolds $C_{r,2}$ (blue) and $C_{a,2}$ (red) in $y_2 = 0$ near a pitchfork bifurcation at $\mu = 2$; furthermore a turning point bifurcation (TPB) is observed at $\mu \approx 1.9985$

By the symmetry properties given by σ_2 the turning point bifurcation happens when the turning point crosses the x_2 axis in the section $y_2 = 0$. Figure 10 shows a graph of the turning point position over the parameter μ in $y_2 = 0$. The first three bifurcation values close to $\mu = 3, 5, 7$ can be seen. These two bifurcations, the transcritical and turning point bifurcation, are always observed near an odd μ.
Figure 11 shows a numerically observed pitchfork bifurcation at $\mu = 2$ where the bifurcating branches exist for $\mu < 2$. Again we observe close by a turning point bifurcation for $\mu \approx 1.999$. Thus the two secondary canards which bifurcate from $\mu = 2$ exist just for a tiny parameter interval. Again, these two bifurcations, the pitchfork and turning point bifurcation, are always observed near an even μ. Hence we have an alternation of transcritical and pitchfork bifurcation for $\mu \in \mathbb{N}$ with nearby turning point bifurcation.
In Figure 12 we summarize these partly analytical, partly numerical results in a bifurcation diagram for (the extensions of) singular canards in chart κ_2. This gives a complete picture of the existence of secondary singular canards. Note that the primary canard γ_2 serves as an organizing center for the

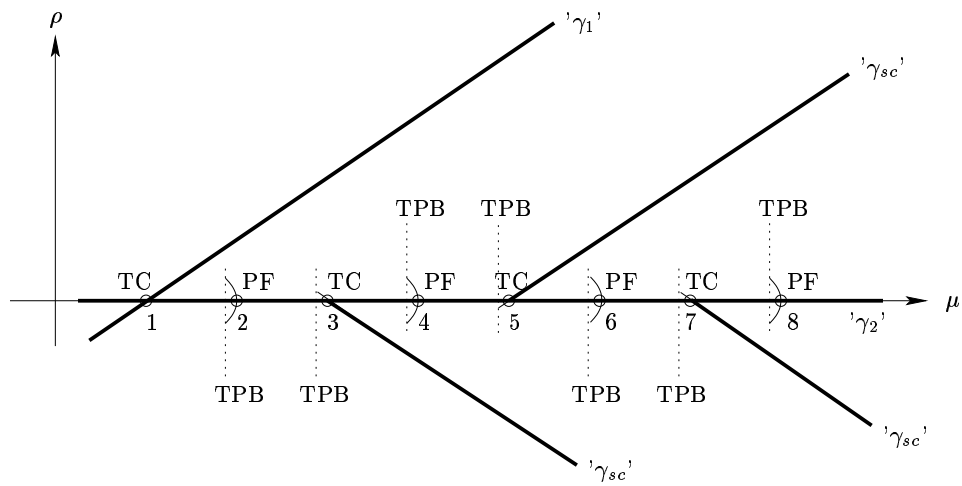

Figure 12: bifurcation diagram for singular canards in κ_2: transcritical (TC), pitchfork (PF) and turning point (TPB) bifurcations; primary canards $\gamma_{1/2}$, secondary canards γ_{sc}; distance ρ with respect to primary canard γ_2.

rotation of the invariant manfolds $C_{r,2}$ resp. $C_{a,2}$. Their rotation number increases monotonically with μ. A secondary canard bifurcates for $\mu \geq \mu_0$, where μ_0 is odd, and is positioned between the two primary canards γ_1 and γ_2. This secondary canard γ_{sc} rotates $\mu_0 \cdot \pi$ times around γ_2. Furthermore a secondary canard does not change its rotation properties after bifurcation with increasing μ. It is 'released' from the organizing center γ_2 but 'captured' by the stable primary canard γ_1 resp. previously bifurcated secondary canards. All these secondary canards are well seperated by an rotation angle of 2π due to the monotonically increasing rotation number of the organizing center. Thus they cannot by annihilated or create new canards by interactions, i.e. there are no more bifurcations. They are stable objects with a well defined distance.
Another observation which distinguish secondary canards from primary canards besides their rotational properties is the following. Note that the secondary canards γ_{sc} originate from the node $P^-_{\lambda_1}$ in $C_{a,1}$ as well as the primary canard γ_1 (see Figure 13). But on the blown-up critical manifold $S_{a,1}$ the sector of singular canards is attracted to $P^-_{\lambda_2}$. Thus the secondary canards have a discontinous decomposition in the invariant sub-manifolds $S_{a,1}$ and $C_{a,1}$ of $M_{a,1}$ while the primary canards have

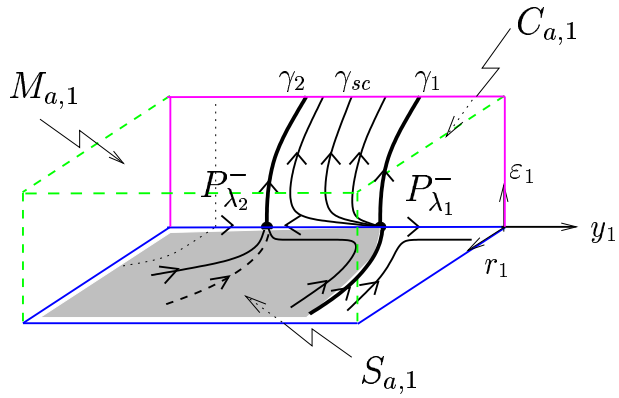

Figure 13: secondary canards on invariant manifold $C_{a,1}$ for e.g. $\mu = 8.5$

a continous decomposition. Thus for small perturbations $0 < \varepsilon \ll 1$ the trajectories of the maximal secondary canards in $M_{a,1}$ are influenced by both saddle points $P^-_{\lambda_1}$ and $P^-_{\lambda_2}$.
The unfolding under small perturbations of the bifurcation diagram 12 depends on the higher order terms $O(r_2)$ in (19). The unfolding of transcritical and pitchfork bifurcation is well covered by singularity theory but the unfolding of the turning point bifurcation is not known and complex behaviour and interaction with the nearby bifurcation points is expected. We are not addressing this subtle issue in this work. The only conclusion we make in this general setting is the following. There exist no branches of secondary singular canards outside a neighbourhood of a pitchfork bifurcation and there exists just one branch of secondary singular canards outside a neighbourhood of a transcritical bifurcation. We denote by U the union of neighbourhoods of bifurcation points. Outside U the branches of secondary canards of the transcritical bifurcations exist and the associated manifolds $C_{r,2}$ and $C_{a,2}$ have a transverse intersection along these secondary canards. Hence they persist as maximal secondary canards under small perturbations. The assertion of Proposition 4.1 follows. We give numerical evidence of the statement for $\mu = 8.5$ in Figure 14 and for $\mu = 14.5$ in Figure 15. Furthermore we observe the rotational properties of the invariant manifolds stated in Proposition 2.5.

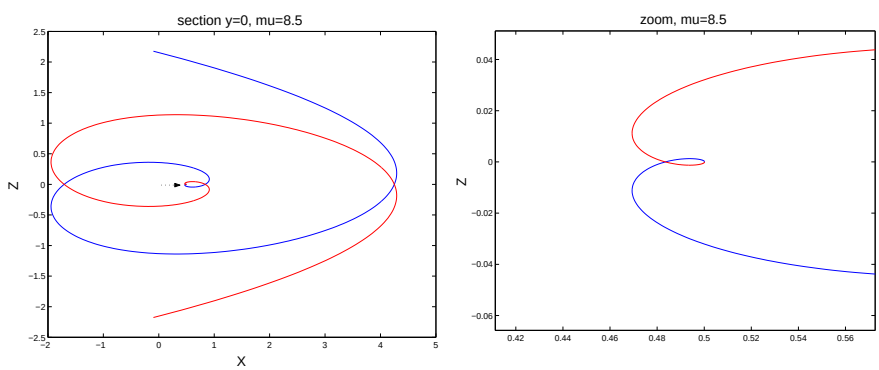

Figure 14: intersection of manifolds $C_{r,2}$ (blue) and $C_{a,2}$ (red) in $y_2 = 0$ for $\mu = 8.5$ with 3 secondary canards (the arrow indicates the zoom)

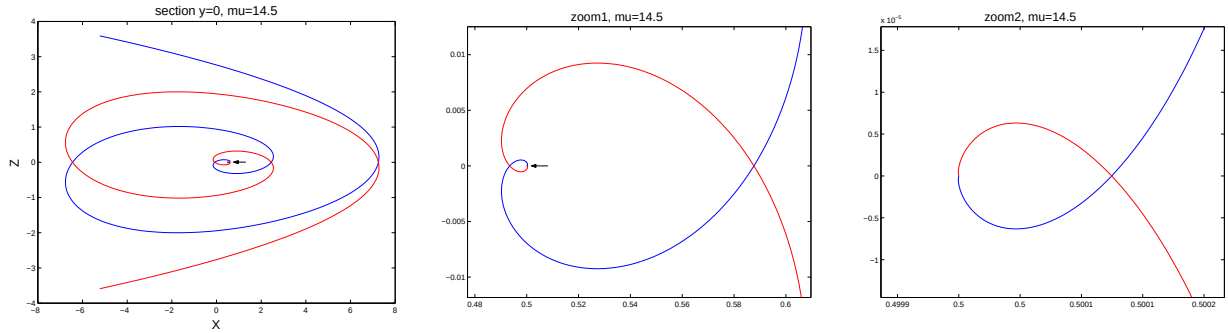

Figure 15: intersection of manifolds $C_{r,2}$ (blue) and $C_{a,2}$ (red) in $y_2 = 0$ for for $\mu = 14.5$ with 6 secondary canards (the arrows indicate the two consecutive zooms)

5 Canards in a synchronized network of Hodgkin-Huxley neurons

Drover at al [DRSE03] studied numerically a network of Hodgkin-Huxley (HH) neurons which are coupled by excitatory synapses. The individual neurons are intrinsically active (through current injection) with high firing rate of about 100 Hz. After the synaptic coupling is turned on the network rapidly synchronizes and fires at a frequency of only about 10 Hz. Stronger coupling, i.e. a higher synaptic conductance, or a longer decay rate of the synapses lead to even lower frequencies. We are showing that canards of folded node type are responsible for this phenomenon.
Since synchrony appears to be a stable state of the network it is sufficient to study a single self coupled HH neuron. The network contains only three currents: a transient sodium current, a potassium current (delayed rectifier) and a leak. A standard procedure reduces the four variable HH model to a two variable reduced HH model (see e.g. [Rin85]). The resulting single self-coupled reduced HH neuron is given by

$$
\begin{aligned}
C\,V' &= -g_{Na}\,h\,m_\infty^3(V)(V-V_{Na}) - g_K\,n^4(h)(V-V_K) - g_L(V-V_L) \\
&\quad + g_{syn}s(V-V_{syn}) + I_{app} \\
h' &= (h_\infty(V)-h)/\tau_h(V) \\
s' &= \alpha(V)(1-s) - s/\tau_{syn}\,,
\end{aligned}
\tag{72}
$$

with voltage V, $h \in [0,1]$ the inactivation of the sodium channels and $s \in [0,1]$ the synaptic coupling. For the definitions of the parameters and functions in (72) we refer to Appendix A of [DRSE03]. Figure 16 shows a simulation of the HH neuron (72) with a decay rate of the synapse $\tau_{syn} = 10$ msec which shows the phenomenon of lowering the frequency from 100 Hz to 10 Hz due to the synaptic coupling. Note the occurance of small oscillations before the neuron fires an action potential.
An important observation is that the decay rate τ_{syn} of the synapse s and the decay rate $\tau_h(V)$ of the inactivation of the sodium channel h are of the same order (5-10 msec). The evolution of h and the deactivation of s are slow compared to the evolution of the voltage V. Thus system (72) can be viewed as a singularly perturbed system.
In the following we study a FitzHugh-Nagumo (FHN) model which has the same qualitative features as the HH neuron but has a simpler and dimensionless form to analyse. The self-coupled FHN model is given by

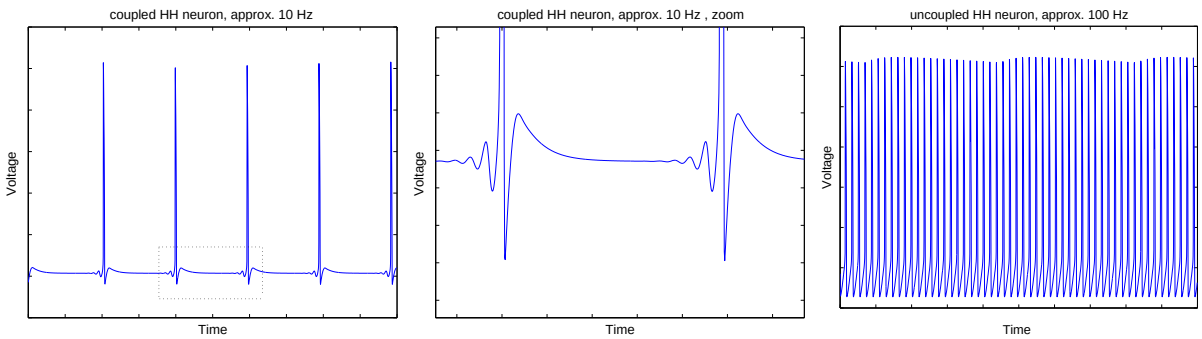

Figure 16: simulation of HH neuron (72) with excitatory synapse (self-coupled), the decay rate of the (slow) synapse is $\tau_{syn} = 10$ msec, the uncoupled neuron fires with about 100 Hz while the self-coupled neuron fires with about 10 Hz

$$
\begin{aligned}
v' &= h - (v^3 - v + 1)/2 - \gamma s v \\
h' &= -\varepsilon(2h + 2.6v) \\
s' &= \alpha(1 - s)H(v) - \varepsilon\delta s\,,
\end{aligned}
\tag{73}
$$

where $H(v)$ is the Heavyside function, γ the coupling rate, α the activation rate, δ the decay rate of the synapse and $\varepsilon \ll 1$ the singular perturbation parameter. Note that the synapse s is slow in the silent phase $v < 0$ while it is fast in the active phase $v > 0$. This is a physiological property of a slow synapse. Figure 17 shows a simulation of the FHN neuron which shows qualitatively the same behaviour as the HH neuron in Figure 16. To understand the slowing of the firing rate we

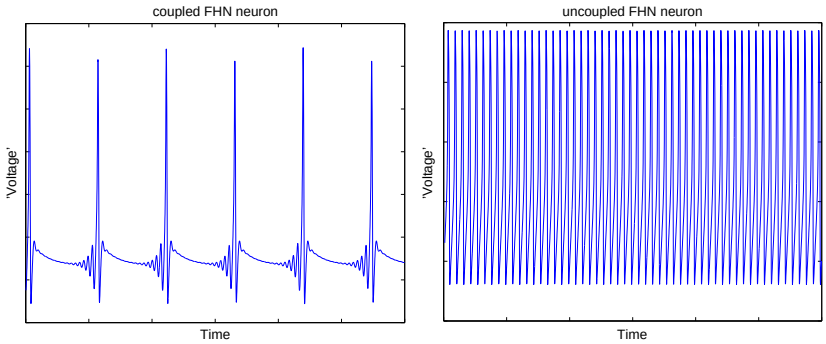

Figure 17: Simulation of FHN neuron (73) with excitatory synapse (self-coupled), the activation rate of the synapse is $\alpha = 0.2$ the (slow) decay rate of the synapse is $\delta = 0.6$, the synaptic coupling strength is $\gamma = 0.5$ and singular perturbation parameter $\varepsilon = 0.015$; the uncoupled neuron ($\gamma = 0$) fires about 10 times faster as the self-coupled neuron

have to study the FHN neuron in the silent phase $v < 0$ where the model is given by

$$
\begin{aligned}
v' &= h - (v^3 - v + 1)/2 - \gamma s v \\
h' &= -\varepsilon(2h + 2.6v) \\
s' &= -\varepsilon\delta s\,,
\end{aligned}
\tag{74}
$$

which is of the form (1) and fits our framework. The critical manifold S of system (74) is given by $h = \varphi(v,s) = (v^3 - v + 1 + 2\gamma s v)/2$ which is a folded manifold for $v < 0$, $s \in (0,1)$ and $\gamma < 0.5$.

Remark: Drover at al [DRSE03] analysed a similar model for the silent phase but the synapse s is not explicitely evolving on a slow time scale. Furthermore they focus on the evolution of the variables (v,h) and view the synapse s like a parameter instead of a second slow variable. This is mainly because they are comparing their results with the classical 2d literature on delayed Hopf bifurcation and canards. We want to emphasize that canards are just generic objects in systems with two (or more) slow variables and thus should be treated in a framework like system (74).

The desingularized reduced system of (74) is given by

$$\begin{aligned} \dot{v} &= -(v^3 - v + 1 + 2\gamma s v) - 2.6v + \gamma\delta v s \\ \dot{s} &= -\delta s(3v^2 - 1 + 2\gamma s)/2\,. \end{aligned} \tag{75}$$

We are looking for singularities of system (75) on the fold-curve $s = \psi(v) = (1 - 3v^2)/2\gamma$ for $v < 0$ and $0 < s < 1$. This leads to solving the cubic equation

$$(3\delta/2 - 2)v^3 + (2.6 - \delta/2)v + 1 = 0\,.$$

This equation has for all $\delta \geq 0$ a real solution $v < 0$ such that $0 \leq \psi(v) \leq \bar{s}_\gamma$ where $\bar{s}_\gamma < 1$ for $\gamma > \bar{\gamma} \approx 0.185$. Figure 18 shows for fixed coupling strength $\gamma = 0.5$ the coordinates (s,v) of the singularity. Further analysis shows that these singularities are canard points of folded node type

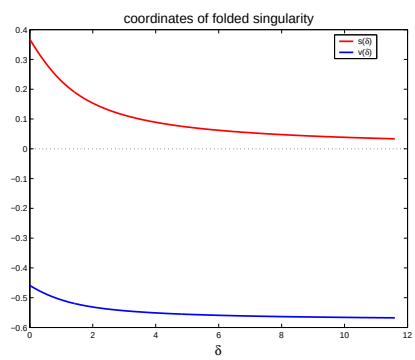

Figure 18: coordinates of the folded singularity in the reduced problem for coupling strength $\gamma = 0.5$ as a function of the synaptic decay rate δ (obtained analytically by Maple).

for $0 \leq \delta < \bar{\delta}(\gamma)$ with e.g. $\bar{\delta}(0.5) \approx 8.72$. Thus the theory of the previous sections applies to this problem. Figure 19 shows the evolution of the synapse s and the voltage v (same parameter values as in Figure 17). Note that a reset of the synapse to a value $s \approx 0.81$ after an action potential occurs which is due to the fast dynamics in the active phase. Furthermore Figure 19 shows the associated reduced flow near the fold-curve in the silent phase. A trajectory enters the silent phase inside the sector between the two primary canards of the folded node (dotted area). From Proposition 4.1 follows the existence of $[(\mu - 1)/2]$ secondary weak canards within the dotted sector (in this case $[(52.4 - 1)/2] = 25$). These secondary canards divide this sector into $([(\mu - 1)/2] + 1)$ sub-sectors. Thus a trajectory enters the silent phase in one of these sub-sectors, gets quickly attracted to the

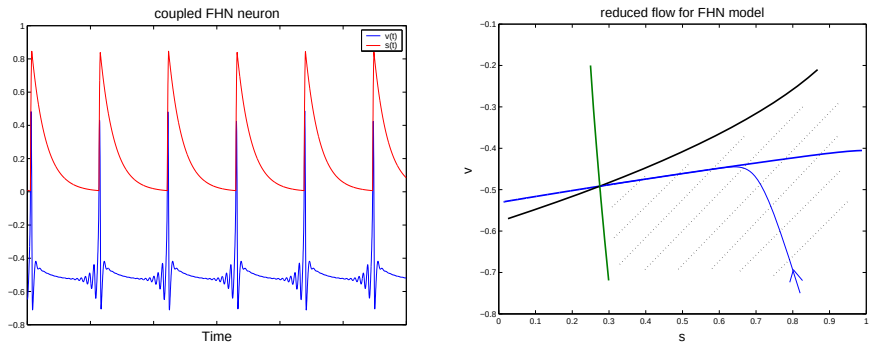

Figure 19: A: evolution of s (red) and v (blue) of the FHN model, same parameters as in Figure 17; B: reduced flow (blue) near singularity of folded node type, strong canard (bold green), primary weak canard (bold blue), fold-curve (black) and sector of weak canards (dotted area)

primary weak canard, follows the primary canard and passes close to the canard point near the fold-curve. The numerical analysis in Section 4 showed that the attracting and repelling manifold form a 'funnel' along the primary weak canard (see Figures 14-15). Thus the trajectory rotates a certain amount of time (depending on the secondary canards of the initial sub-sector) around the primary weak canard before it gets repelled and finally fires an action potential. This behaviour is robust and explains qualitatively the observed delay in the firing of the FHN neuron (73) resp. the HH neuron (72).

Remark: This folded node structure embedded in the FHN neuron explains the 'novel vortex structure' observed by Drover at al [DRSE03].

We want to point out that the periodic patterns created by the canards of folded node type in the FHN resp. HH model are mixed mode oscillations (MMO). This becomes more apparent if the resonance parameter μ is not so large. Figure 20 shows 1^0-1^5 MMO patterns where $\mu \approx 9.9$ for all six patterns where the parameters correponding to the silent phase are fixed. We are just varying the activation rate α of the synapse. Thus we are changing the 'initial condition' for the trajectory entering the silent phase. We have 4 secondary canards which divides the sector between the two primary canards into 5 sub-sectors (see Figure 21). For small values of the activation rate α we enter the silent phase to the left of the primary strong canard (outside the sector) and we are in the relaxation regime which corresponds to the MMO pattern 1^0. With increasing α trajectories enter the sub-sectors between the primary strong and weak canard. Remember that the secondary canards are well seperated by an rotation angle of 2π. Thus depending on the sub-sector where the trajectory is initially positioned we obtain $1^1 - 1^5$ MMO patterns. These patterns are generically robust under small perturbations. Just in the transition from one to another sub-sector chaotic behaviour has to be expected. A detailed study of MMO patterns in systems with folded nodes is part of future work.

Remark: Another class of problems where MMO occur are systems with canard points of folded saddle-node type (type II). A geometric analysis for this class of MMO can be found in [BKW03]. For an application we refer to the study of a 3d chemical autocatalator by Milik et al [MSLG98].

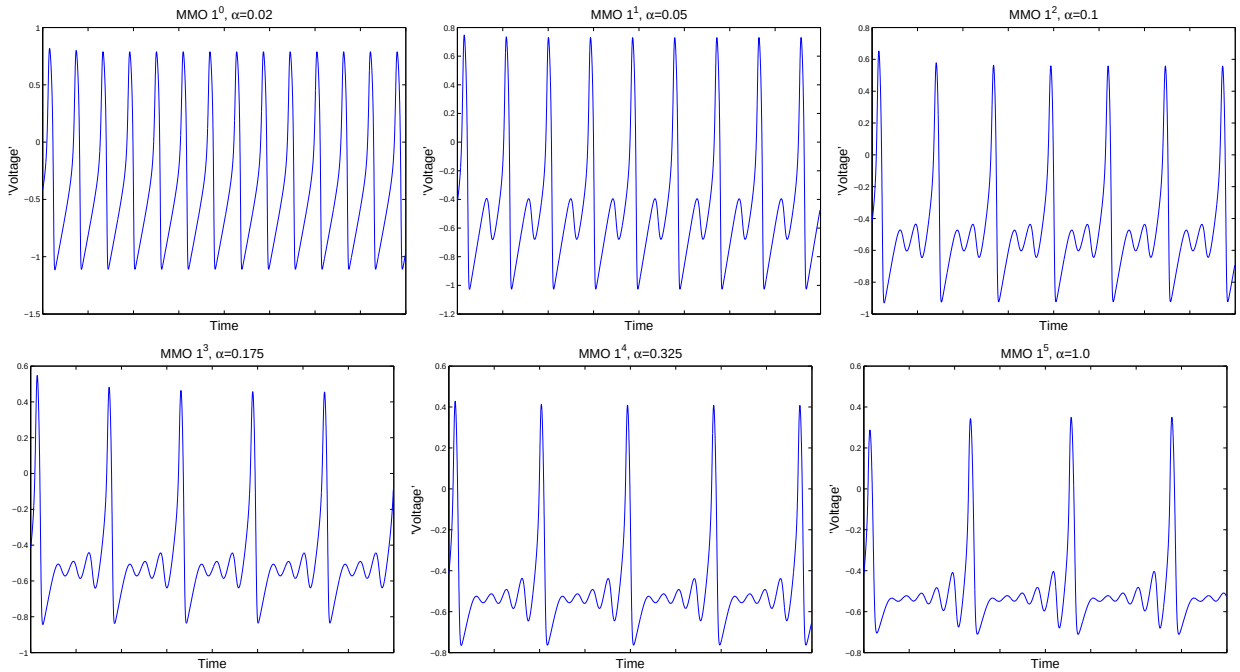

Figure 20: Mixed Mode Oscillations (MMO) with 1^0-1^5 pattern in the FHN model (73) by variation of activation rate α

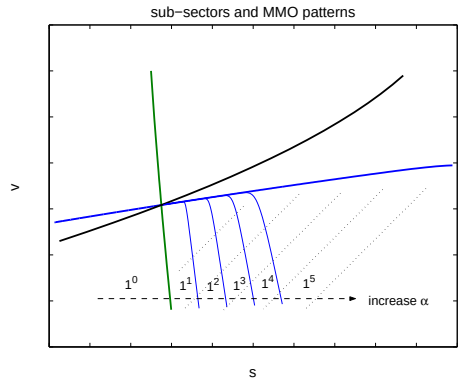

Figure 21: secondary canards (blue), primary strong (bold green) and primary weak canard (bold blue), fold-curve (black) and sector of weak canards (dotted area); secondary canards divide sector into sub-sectors which represent the domain of the MMO patterns $1^1 - 1^5$ of Figure 20

References

[Arn81] V. I. Arnold [1981]. *Singularity Theory*. London Mathematical Society Lecture Notes Series, 53, Cambridge University Press, Cambridge.

[Ben83] E. Benoît [1983]; *Systémes lents-rapides dans* $\mathbb{R}^3$ *et leur canards*; Asterisque **109-110**, 159-191.

[Ben90] E. Benoît [1990]; *Canards et Enlacements*; Publications de l'Inst. des Hautes Etudes Scient. **72**, 63-91.

[Ben01] E. Benoît [2001]; *Perturbation singuliére en dimension trois: canards en un point pseudo- singulier noeud*; Bull. Soc. Math. France **129**, 1, 91-113.

[BKW03] M. Brøns, M. Krupa and M. Wechselberger [2003]; *Mixed mode oscillations and canards of folded saddle-node type*, in preperation.

[DRSE03] J. Drover, J. Rubin, J. Su and B. Ermentrout [2003]; *Analysis of a canard mechanism by which excitatory synaptic coupling can synchronize neurons at low firing frequencies*; preprint.

[DR96] F. Dumortier, R. Roussarie [1996]; *Canard cycles and center manifolds*; Memoires of the AMS **557**.

[Fen79] N. Fenichel [1979]; *Geometric singular perturbation theory*; JDE **31**, 53-98.

[GS84] M. Golubitsky, D. Schaeffer [1984]; *Singularities and groups in bifurcation theory*; Applied mathematical sciences **51**, Springer Verlag, New York.

[GH03] J. Guckenheimer, R. Haiduc [2003]; *Canards at folded nodes*; preprint.

[HMM95] D. Hansel, G. Mato and C. Meunier [1995]; *Synchrony in excitatory neural networks*; Neural Computation **7**, 307-337.

[Jon95] C.K.R.T. Jones [1995]; *Geometric singular perturbation theory*; in Dynamical Systems, Springer Lecture Notes Math. **1609**, 44-120.

[KS99] M. Krupa, P. Szmolyan [1999]; *Extending geometric singular perturbation theory to nonhyperbolic points - fold and canard points in two dimensions*; SIAM J. of Math. Anal. **33** (2),286-314.

[MSLG98] A. Milik, P. Szmolyan, H. Löffelmann, E. Gröller [1998]; *The geometry of mixed-mode oscillations in the 3d-autocatalator*; International Journal of Bifurcation and Chaos **8**, 505-519.

[MKKR94] E.F. Mishchenko, Yu.S. Kolesov, A.Yu. Kolesov, N.Kh. Rhozov [1994]; *Asymptotic methods in singularly perturbed systems*, Monographs in Contemporary Mathematics; Consultants Bureau, New York, A Division of Plenum Publishing Cooperation 233 Spring Street, New York, N.Y. 10013.

[Rin85] J. Rinzel [1985]; *Excitation dynamics: insights from simplified membrane models*, Fed. Proc. **44**, 2944-2946.

[SW01] P. Szmolyan, M. Wechselberger [2001]; *Canards in* $\mathbb{R}^3$; JDE **177**, No.2, 419-453.

[Wec02] M. Wechselberger [2002]; *Extending Melnikov-Theory to invariant manifolds on non-compact domains*; Dynamical Systems **17**, No.3, 215-233.

[Wec98] M. Wechselberger [1998]; *Singularly perturbed folds and canards in* $\mathbb{R}^3$; Thesis, Vienna University of Technology, Austria.